GSA DATA REPOSITORY 2016014

Supplementary Information for

Ocean warming not acidification controls coccolithophore response during past greenhouse climate change

Samantha J. Gibbs, Paul R. Bown, Andy Ridgwell, Jeremy R. Young, Alex J. Poulton and Sarah A. O'Dea.

correspondence to: s.gibbs@noc.soton.ac.uk

This PDF file includes:

Supplementary Methods

Suuplementary Figures and Tables

References unique to Supplementary Information

Supplementary Methods

Earth system modeling

We employ 'cGENIE' – an Earth system model of intermediate complexity comprising: a 3-D dynamic ocean circulation model with simplified 'energy and moisture' balance atmosphere (Edwards and Marsh, 2005), a representation of the biogeochemical cycling of elements and isotopes in the ocean (Ridgwell et al., 2007), plus marine sediment (Ridgwell and Hargreaves, 2007) and terrestrial weathering (Colbourn et al., 2013) components in order to close the geological cycle of carbon. In the modern, seasonally-forced version of this model, the (year 1994) anthropogenic CO_2 inventory lies close to observations (Cao et al., 2009) and the specific combination of weathering feedback and marine sediment burial results in a millennial-scale CO_2 response comparable to other Earth system models (Archer et al., 2009).

In an initial spin-up of Eocene ocean circulation and carbon cycling, cGENIE was run for 20 kyr with atmospheric CO_2 set to 834 ppm and its $\delta^{13}C$ to -4.9‰. In this first phase spin-up, as described in Ridgwell and Hargreaves (2007), the ocean-atmosphere carbon cycle was forced 'closed' with weathering tracking sedimentary burial of $CaCO_3$ at all times and no bioturbational mixing in the sediments. In a second follow-on phase of spin-up, the model was run as an 'open' system temperature-dependent silicate and carbonate weathering enabled (Archer et al., 2009; Colbourn et al., 2013). The global Ca^{2+} burial flux (14.48 Tmol Ca^{2+} yr^{-1}) was diagnosed from the end of the 1st spin-up phase and split equally between (calcium) silicate and carbonate weathering. A flux of volcanic CO_2 outgassing of 7.24 Tmol C yr^{-1} (at -6.0 ‰) was specified to balance consumption by silicate weathering and bioturbational mixing of the sediments was now enabled (again, following the procedure of Ridgwell and Hargreaves, 2007). The $\delta^{13}C$ signature of carbonate weathering was set to balance the long-term ^{13}C budget, requiring in the absence of organic carbon deposition, a value of 13.58 ‰. This 2nd spin-up phase was run for 200 kyr with atmospheric CO_2 and $\delta^{13}C$ free to evolve. In a subsequent control experiment, the resulting drift in atmospheric CO_2 was less than 0.2 ppm over 200 kyr.

Finally, in order to extract modelled environmental variables at the paleo locations of the data (Supplementary Information Fig. DR1), modern site locations were converted to 55 Ma paleolatitude and paleolongitude values using the “Point Tracker (v. 7) for Windows” software package (www.scotese.com). However, this plate reconstruction differs from that underlying the cGENIE model continental configuration, which derived from Tindall et al. (2010). We approximately reconciled the two different early Eocene plate reconstructions in the simplest possible way, avoiding extensive by-eye adjustments, by: firstly shifting every data point (Supplementary Fig. DR1) by -10°E (equivalent to a single cGENIE model grid point in longitude). (The absolute longitude of the plates accounts for much of the differences between reconstructions, but fortunately this is something that appears to affect all plates approximately equally). Secondly, for any data location found lying on the model land grid, we adjusted its latitude by either +5 or -5°N (a procedure which was required for: Lodo (-5°N), New Jersey (-5°N), Tanzania (+5°N), Kerguelen (+5°N), and Gebel Serai and Gebel Aweina (+5°N)), which typically results in a latitudinal shift of a single grid model point.

High resolution ECC occurrences

In addition to the meta-analysis, we also documented the stratigraphic duration of the PETM holococcolith gap in detail, using high-resolution distribution data for ECCs from Bass River (new data herein) and South Dover Bridge (Self-Trail et al., 2012), where preservation is exceptional across the PETM, and from ODP Sites 401 (new data) and 690 (new data), which have high abundances of holococcoliths (Supplementary Fig. DR3). The data confirm the presence of the holococcolith gap and demonstrate that it is short-lived and restricted to the onset and into the peak of the event.

Supplementary Figures and Tables

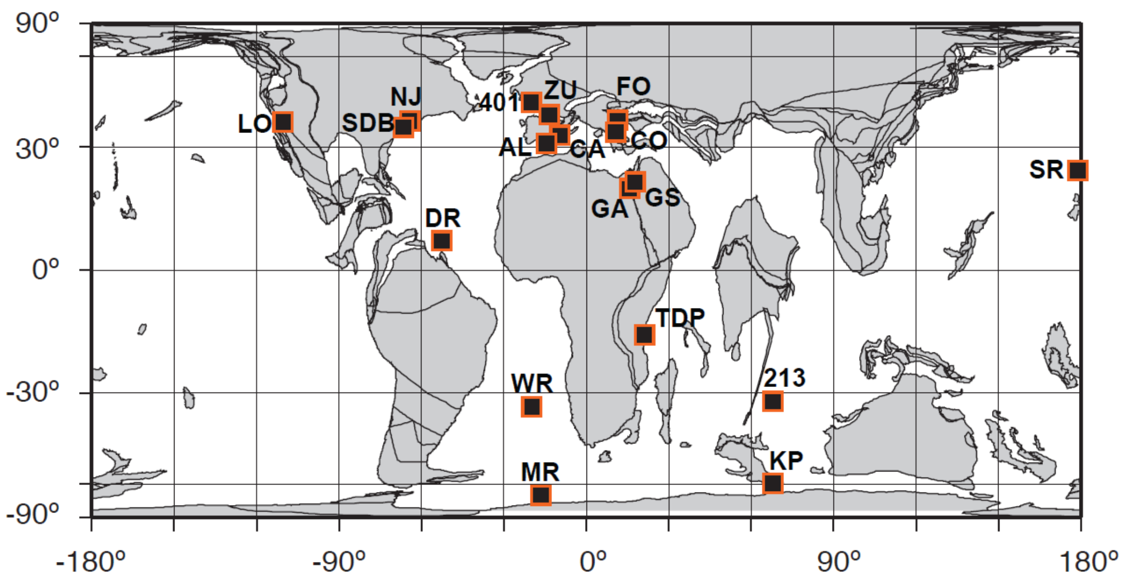

Supplementary Figure DR1. Paleogeographic reconstruction for the Paleocene-Eocene Thermal Maximum with locations of sites included in this study - Lodo Gulch, California (LO, data herein, Table DR1a); South Dover Bridge, Maryland (SDB, ref *a*); New Jersey (NJ – Clayton, ref *b*; NJ GL913, ref *b*; Bass River, ref *c*; Wilson Lake, refs *d*, *c*); ODP Sites 1259 and 1260, Demerara Rise (DR, refs *e*, *f*); ODP Sites 1262 and 1263, Walvis Ridge (WR, ref *g*); ODP Site 690, Maud Rise (MR, ref *c*, *h*); DSDP Site 401, Bay of Biscay (401, data herein, Table DR1b); Zumaia, Spain (ZU, refs *i*, *j*, *k*); Alamedilla, Spain (AL, ref *k*); Caravaca, Spain (CA, ref *l*); Forada, Italy (FO, ref *m*); Contessa, Italy (CO, ref *k*); Gebel Serai, Gebel Aweina, Egypt (GS, GA, ref *n*); Kilwa, Tanzania Drilling Project corehole 14a, Tanzania (TDP, ref *o*); DSDP Site 213, Indian Ocean (213, ref *p*); ODP Site 1135, Kerguelen Plateau (KP, ref *q*), and ODP Site 1209, Shatsky Rise (SR, refs *c*, *d*). References are listed at the end of the supplementary information.

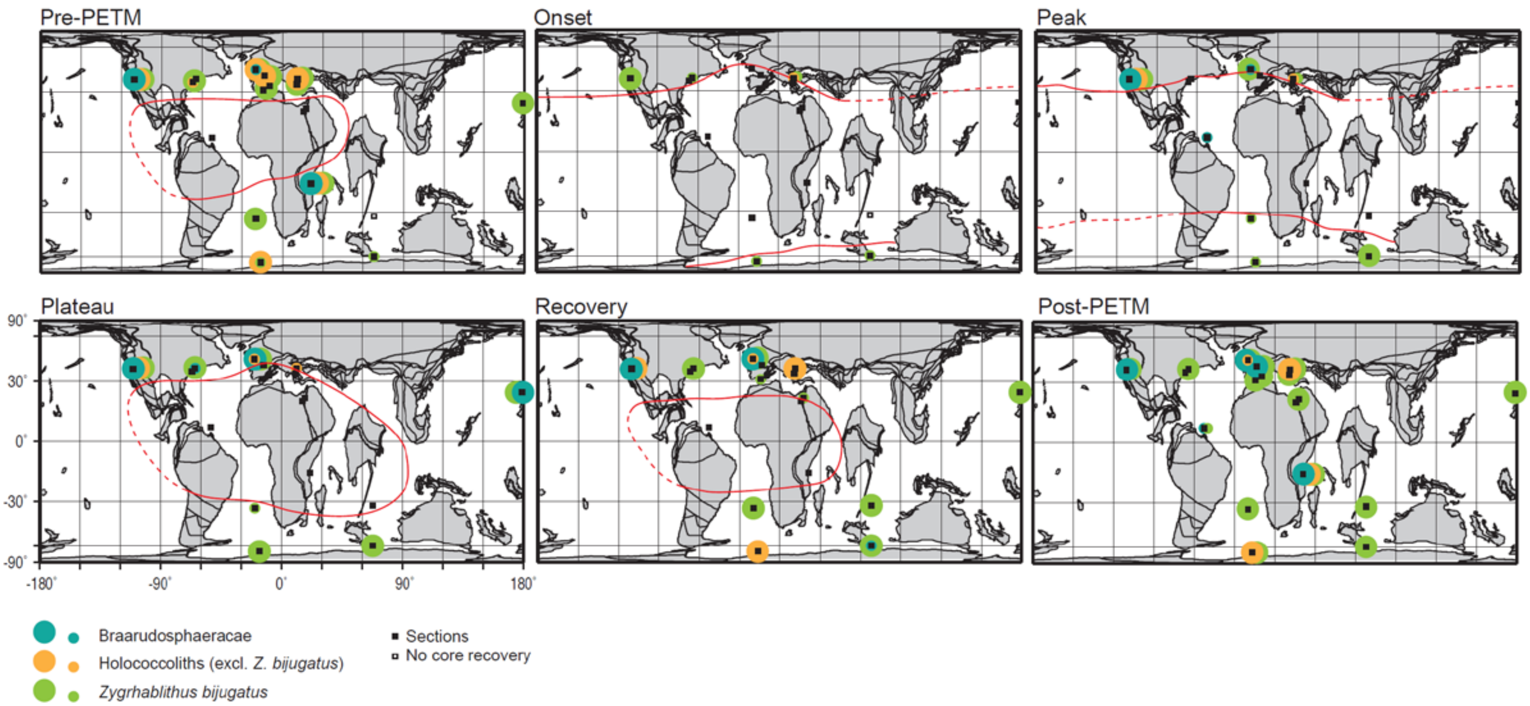

Supplementary Figure DR2. ECC occurrence for PETM time-slices, based on meta-analysis of globally distributed sites. Abundance of the different ECCs (braarudosphaerids, holococcoliths excluding *Zygrhablithus bijugatus*, and *Z. bijugatus*) is illustrated by coloured circles with a larger circle indicating higher relative abundance and a small circle representing low abundance. The red line indicates the approximate geographic area of ECC absence with uncertainly shown with a dashed line. The holococcolith grouping includes the species *Clathrolithus ellipticus*, *Holodiscolithus macroporus*, *Holodiscolithus solidus*, *Lanternithus simplex*, *Munarius emrei*, *Octolithus* spp., *Semihololithus biskayae*, *Semihololithus dimidius* and *Semihololithus kanungoi*.

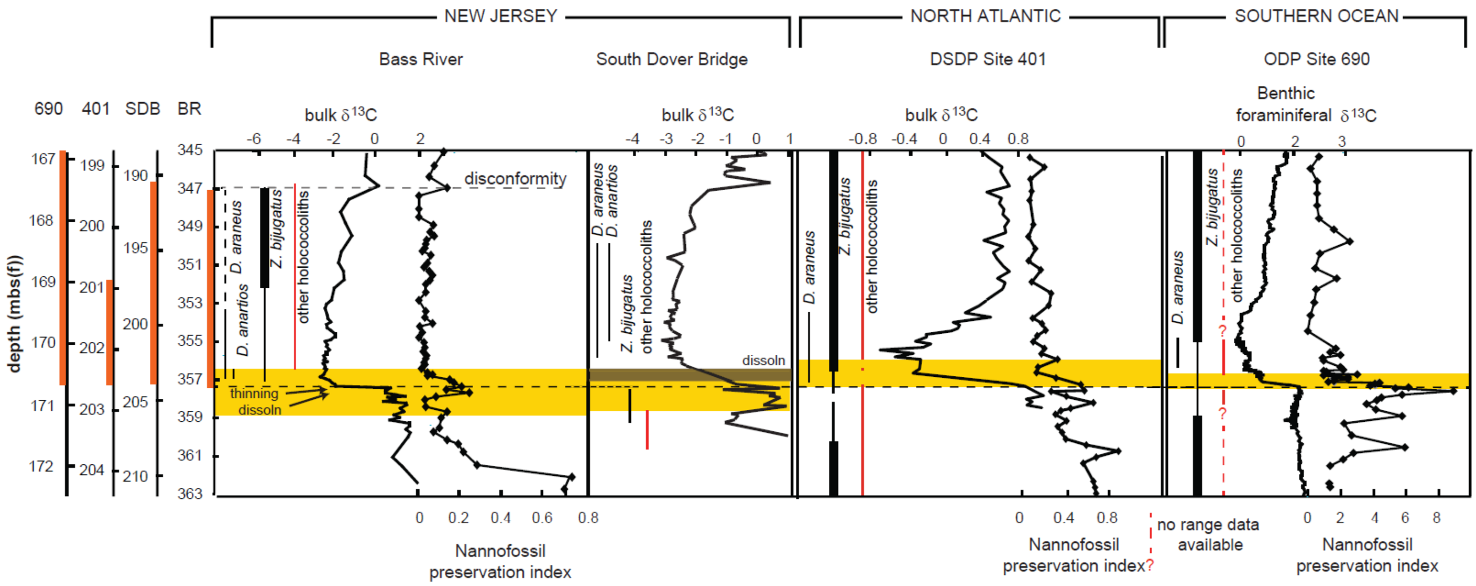

Supplementary Figure DR3. High-resolution records of holococcolith presence across the PETM interval. A. Bass River (BR), data herein, B. South Dover Bridge (SDB), from ref. a, C. DSDP Site 401, data herein, and D. ODP Site 690. Stratigraphic ranges of *D. araneus*, *D. anartios* (both PETM bio-indicators) and *Z. bijugatus* (black lines) and holococcoliths (red lines) are shown, with increased abundance indicated by a thicker line. In a., 'thinning' indicates the level where thinning was observed in *Coccolithus pelagicus* liths in O'Dea et al. (2014) and interpreted as peak surface water OA, and 'dissoln' (dissolution) indicates the level where peak dissolution occurs. Yellow shading indicates the stratigraphic interval across which holococcoliths (excluding *Z. bijugatus)* appear to be mainly absent. $\delta^{13}C$ records are from John et al. (2008), Self-Trail et al. (2012), Nunes and Norris (2006), Bains et al. (1999) in A to D, respectively, and nannofossil preservation indices are from Gibbs et al. (2010) for A and D, and herein for C. CIE extent is indicated on the depth axes (orange shading) and depth scales are metres below surface (mbs) for BR and SDB and metres below seafloor (mbsf) for DSDP Sites 401 and 690.

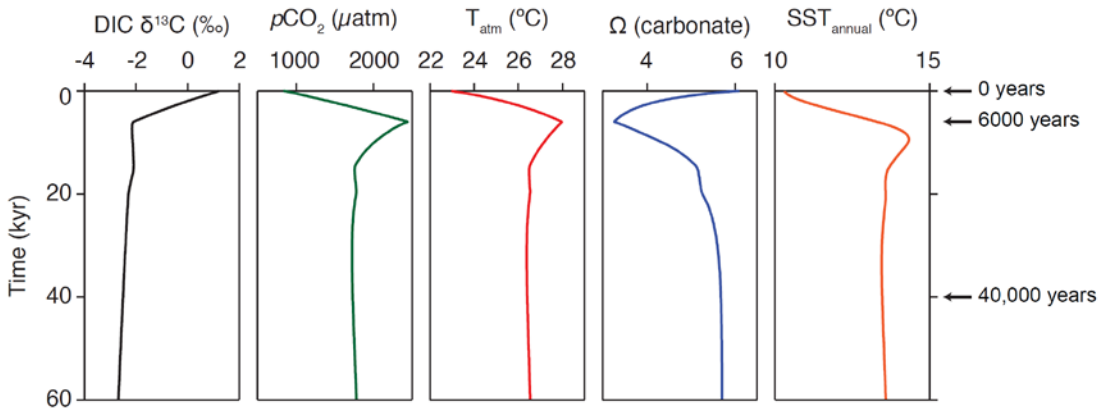

Supplementary Figure DR4. cGENIE Earth system model output $\delta^{13}C$, *p*CO2, atmospheric temperature, carbonate saturation state and sea surface temperature, including the first 60 kyr of the model run. PETM time-slices are indicated as 0 years (pre-CIE), 6,000 years (CIE onset into transient peak) and 40,000 years (CIE plateau).

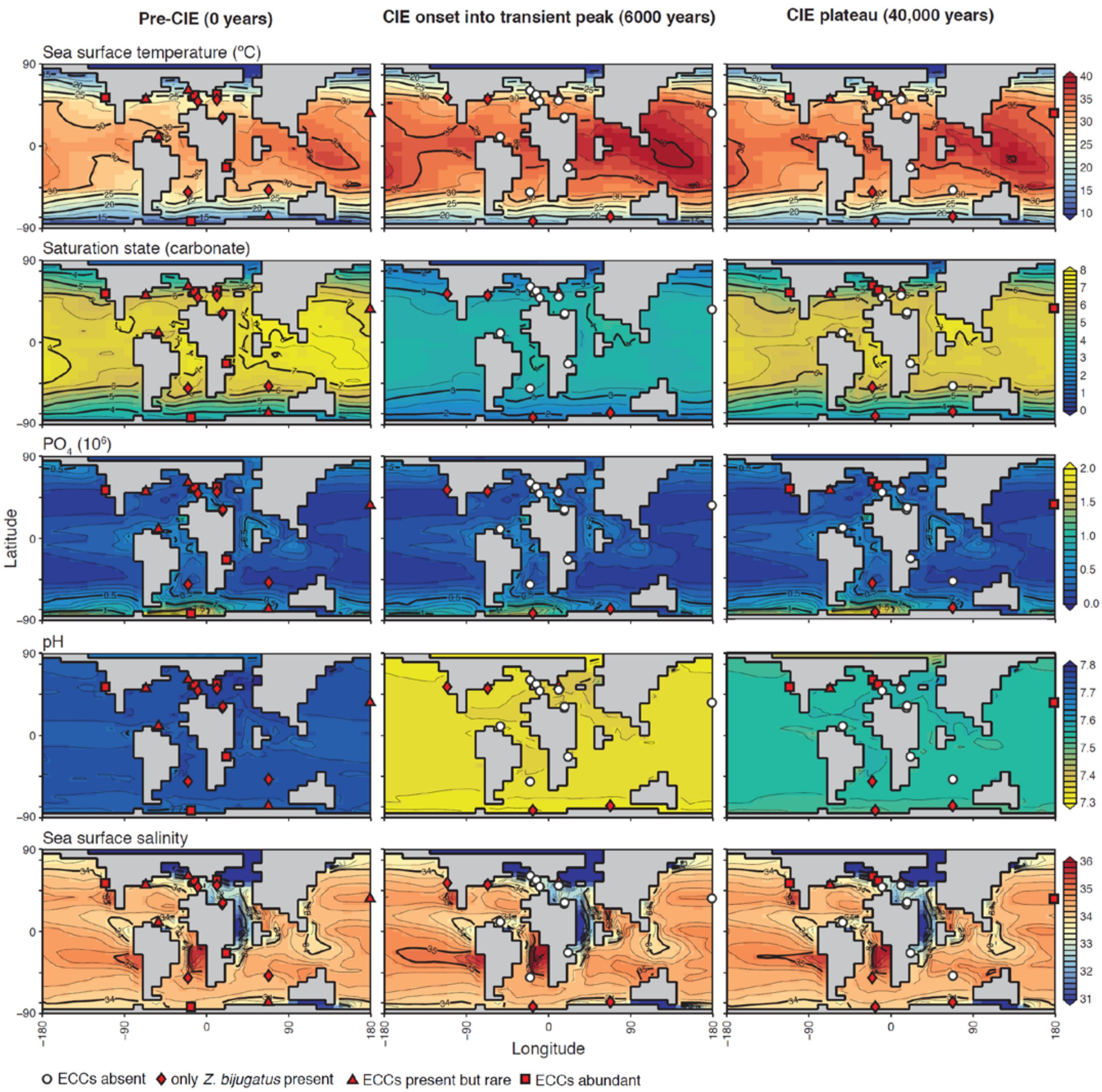

Supplementary Figure DR5. ECC occurrence and cGENIE Earth system model sea surface temperature, saturation state (carbonate), phosphate concentration, pH and sea surface salinity output, at PETM time-slices. ECC occurrence (red symbols) and absence (open circles) for each site is superimposed upon mean annual model outputs for pre-CIE (0 years), CIE onset into transient peak (6,000 years) and CIE plateau (40,000 years). Positions of modelled time-slices relative to the CIE are in Supplementary Fig. 4.

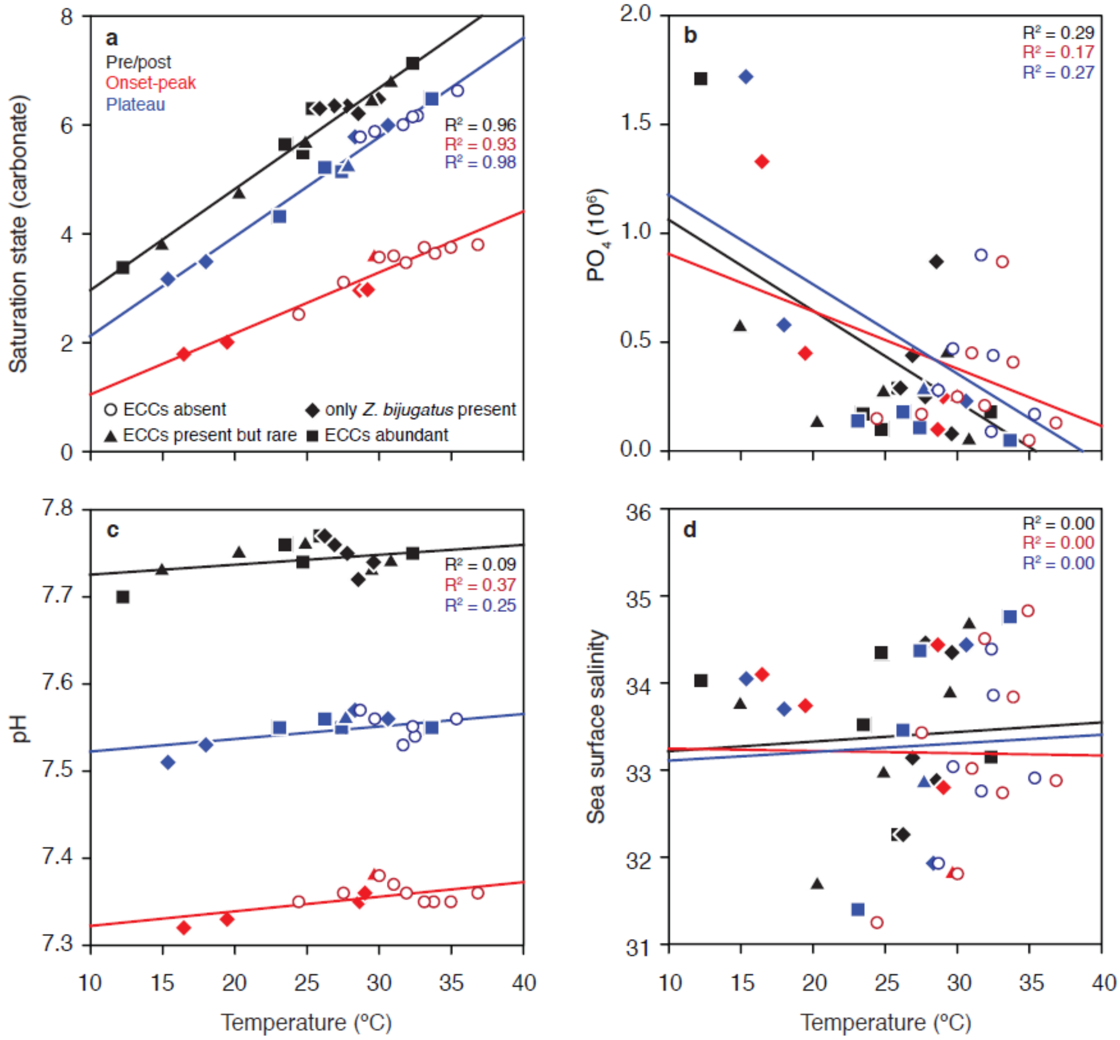

Supplementary Figure DR6. ECC occurrence with cGENIE Earth system model mean annual outputs for environmental parameters, against sea surface temperature (SI Table DR2). A. carbonate saturation state, B. phosphate concentration, C. pH, and D. sea surface salinity. ECC occurrence (closed symbols) and absence (open circles) are shown for each site, with records compiled for pre/post (black), onset-peak (red) and plateau (blue) time-slices (see Supplementary Fig. 2), which correspond to the 0 year, 6,000 year and 40,000 year time-slices used for model outputs (as in Fig. 2), respectively. The linear regression between modelled parameters at each time-slice is shown.

Supplementary Information Table DR1. ECC abundances at DSDP Site 401 and Lodo Gulch.

Table DR1a. Lodo Gulch, California.

LODO GULCH Modern latitude N36°35'46" longitude W120°38'48"

Sample	Stratigraphic height (m)	***Braarudosphaera bigelowii***	***Clathrolithus ellipticus***	***Holodisco. macroporus***	*Holodisco. solidus*	holococcolithus spp.	***Micrantholithus att.***	*M. astrum*	*Micrantholithus bramlettei*	***Zygrhablithus bijugatus***	*Z. nolfii*
LO-03-21	76.77						2				
LO-03-20	73.30							2		F	
LO-03-19	69.67						1			F	1
LO-03-18	65.78	1				2	R			C	1
LO-03-13	45.88				1	2	F			C	1
LO-03-11	39.41									C-F	
LO-03-07	30.70										
LO-03-05	28.00										
LO-03-04	26.50					1					
LO-03-02	23.50	DISCONFORMITY									
LO-03-1A	20.30	C		F	1			F		C-A	
LO-03-40	20.10	F	1		F	F	2		1	F-C	
LO-03-1B	19.00	C	1	2	R			F	1	A	
LO-03-34	18.10	F	F	F	F	F	F		*	C	
LO-03-33	16.60	C	F	F			F			C	
LO-03-32	15.20	C	F	F	*	*	F		*	C	
LO-03-31	13.70	C	F	X	F		R		X	C	
LO-03-37	14.40	F	F	1	F		1	2	1	F	
LO-03-30	12.70	C	F	X	F	X	F			C	
LO-03-29	12.10	F	F	F	F		F			C	
LO-03-28	11.30	F	F	*	F	*	R		R-F	C	
LO-03-27	9.60	C	F-C		F		F			C	
LO-03-27 / +160	9.10	F-C	F		R-F	F	F		R	F	
LO-03-27 / +130	8.80	F	F	R	R	F-R	F		R	F	
LO-03-27 / +110	8.60	F-R	F	R	F	R-F	F		R	F	
LO-03-26A	8.20				F					F	
LO-03-26B	8.15	F					R		R	C	
LO-03-27 / +20	7.70	F-R	F		F	F	F		R	F	
LO-03-27 / +10	7.60	F	F	R	R	F-R	F		VR	F-C	
LO-03-27 / 0	7.50	F-C	F	*	F	F	F		*	F	
LO-03-27 / -10	7.40	F	F	X	R	F	F		R-F	F	
LO-03-27 / -47	7.03	F	F		*	F	F		*	F	
LO-0066	7.80	F	F-R		F-R	1		R	1	F-C	

C - common
F - few
R - rare
VR - very rare
* - seen once

Table DR1b. DSDP Site 401, north Atlantic.

DSDP SITE 401 Modern latitude N47°25'38" longitude W8°48'38"

Percent abundances of total nannofossil assemblage

Sample	Depth (m)	*Semiholithus biscayae*	*S. dimitus?*	*Semiholithus/Z.bij?*	*Semi/Octolithus?*	*Octolithus*	*Holodiscolithus solidus*	*H. macroporus*	*H. serrus*	*Orthozygus?*	*Dakylethra?*	Small, dark holococcolith	Holo simple, grey	Holo ssp.?
14 1 30cm	198.84						0.11	0.14		0.07	0.04	0.18	0.04	0.04
14 1 50cm	199						0.19							
14 1 70cm	199.2						0.18	0.09					0.23	
14 1 90cm	199.4						0.18						0.15	
14 1 105cm	199.55						0.21						0.16	
14 1 145cm	199.95						0.08						0.04	
14 2 15cm	200.15						0.08	0.04					0.08	
14 2 35cm	200.35						0.05							0.05
14 2 55cm	200.55						0.23	0.07					0.03	
14 2 70cm	200.7						0.17							
14 2 90cm	200.9						0.33	0.19					0.14	
14 2 109cm	201.09						0.1			0.05				0.05
14 2 129cm	201.29	0.05					0.4	0.25					0.15	
14 3 0cm	201.5						0.11	0.11		0.05				
14 3 9cm	201.59						0.1	0.05						
14 3 20cm	201.7													
14 3 29cm	201.79						0.2			0.07				
14 3 39cm	201.89						0.13							
14 3 50cm	202						0.25							
14 3 59cm	202.09					0.04	0.18		0.04					
14 3 69cm	202.18				0.04									
14 3 81cm	202.31													
14 3 90cm	202.4						0.14							
14 3 99cm	202.49													
14 3 110cm	202.6	0.36			0.41	0.09								
14 3 120cm	202.7	0.25			0.66									
14 3 121cm	202.71	0.44	0.13		0.22	0.13								
14 3 129cm	202.79	0.7			1.16									
14 3 140cm	202.9	1.33	0.67	0.89	2.44	0.67								
14 3 149cm	202.99	1.25	0.13		1	0.75								0.13
14 4 3cm	203.03	4.31	0.2	0.78	1.76	1.37	0.39							
14 4 9cm	203.09	6.43		0.36	3.57	1.07								
14 4 20cm	203.2	7.78		0.74	3.7	0.37								
14 4 29cm	203.29	8.89			2.86	0.32								
14 4 39cm	203.39	2.3		0.41	2.03	0.14								
14 4 50cm	203.5	1.53			1.31									0.11
14 4 60cm	203.6	2.39	0.22	0.22	2.17	0.43								
14 4 70cm	203.7	1.18		0.26	1.44	0.39								
14 4 80cm	203.8	3.08		0.51	4.1	1.03								
14 4 90cm	203.9	2.6		0.4	3.8	0.8								
14 4 120cm	204.2	3.55		0.32	1.94	0.65								
14 4 130cm	204.3	3.33		0.33	3	0.67								
14 4 140cm	204.4	3.08		0.58	1.92	0.19								

Supplementary Information Table DR2. Data used in SI Figure DR6.

Pre/Post CIE:

Site label	paleo long	paleo lat	ECC occurrence*	Sea surface temperature (ºC)	Saturation state (carbonate)	PO4 (10^6)	pH	Sea surface salinity
LO	-111	36.1	1	24.73	5.49	0.10	7.74	34.35
NJ	-66.7	34.7	2	24.89	5.66	0.27	7.76	32.96
DR	-52.8	6.5	2	29.49	6.43	0.45	7.73	33.88
WR	-20.5	-34	3	27.79	6.35	0.25	7.75	34.43
MR	-17.2	-65.7	1	12.24	3.38	1.71	7.70	34.03
TDP	21.4	-14.9	1	32.32	7.13	0.18	7.75	33.15
KP	67.6	-58.9	2	14.95	3.78	0.57	7.73	33.75
SR	-181.1	23.6	2	30.82	6.77	0.05	7.74	34.67
GA	17.1	19.7	3	28.56	6.21	0.87	7.72	32.88
GS	17.6	20.6	3	28.56	6.21	0.87	7.72	32.88
401	-20.2	42.5	2	20.29	4.72	0.13	7.75	31.68
ZU	-13.4	38.3	1	23.48	5.64	0.17	7.76	33.52
AL/CA	-9.7	32.9	3	26.90	6.35	0.44	7.76	33.14
CO	11.2	34.4	3	25.89	6.30	0.29	7.77	32.26
FO	11.2	37	1	25.89	6.30	0.29	7.77	32.26
213	67.8	-32.3	3	29.62	6.47	0.08	7.74	34.35

CIE onset:

Site label	ECC occurrence*	Sea surface temperature (ºC)	Saturation state (carbonate)	PO4 (10^6)	pH	Sea surface salinity
LO	3	28.65	2.96	0.10	7.35	34.44
NJ	3	29.03	3.02	0.25	7.36	32.80
DR	4	33.87	3.64	0.41	7.35	33.84
WR	4	31.86	3.47	0.21	7.36	34.51
MR	3	16.47	1.79	1.33	7.32	34.10
TDP	4	36.84	3.80	0.13	7.36	32.88
KP	3	19.47	2.01	0.45	7.33	33.74
SR	4	34.97	3.74	0.05	7.35	34.83
GA	4	33.13	3.75	0.87	7.35	32.74
GS	4	33.13	3.75	0.87	7.35	32.74
401	4	24.43	2.52	0.15	7.35	31.25
ZU	4	27.53	3.11	0.17	7.36	33.43
AL/CA	4	31.01	3.58	0.45	7.37	33.02
CO	4	30.01	3.57	0.25	7.38	31.81
FO	2	30.01	3.57	0.25	7.38	31.81
213	No data					

CIE Plateau:

Site label	paleo long	paleo lat	ECC occurrence*	Sea surface temperature (ºC)	Saturation state (carbonate)	PO4 (10^6)	pH	Sea surface salinity
LO	-111	36.1	1	27.41	5.14	0.11	7.55	34.40
NJ	-66.7	34.7	2	27.69	5.22	0.28	7.56	32.85
DR	-52.8	6.5	4	32.49	6.17	0.44	7.54	33.86
WR	-20.5	-34	3	30.62	5.99	0.23	7.56	34.44
MR	-17.2	-65.7	3	15.37	3.17	1.72	7.51	34.05
TDP	21.4	-14.9	4	35.36	6.63	0.17	7.56	32.91
KP	67.6	-58.9	3	18.00	3.49	0.58	7.53	33.70
SR	-181.1	23.6	1	33.66	6.48	0.05	7.55	34.76
GA	17.1	19.7	4	31.66	5.99	0.90	7.53	32.76
GS	17.6	20.6	4	31.66	5.99	0.90	7.53	32.76
401	-20.2	42.5	1	23.11	4.32	0.14	7.55	31.40
ZU	-13.4	38.3	1	26.24	5.22	0.18	7.56	33.46
AL/CA	-9.7	32.9	4	29.70	5.88	0.47	7.56	33.04
CO	11.2	34.4	4	28.69	5.78	0.28	7.57	31.93
FO	11.2	37	3	28.69	5.78	0.28	7.57	31.93
213	67.8	-32.3	4	32.36	6.15	0.09	7.55	34.39

***ECC occurrence**

Number	Description	Symbol
1	Abundant	Square
2	Present but rare	Triangle
3	only *Z. bijugatus* present	Diamond
4	Absent	Circle

References unique to Supplementary Information

Archer, D., Eby, M., Brovkin, V., Ridgwell, A., Cao, L., Mikolajewicz, U., Caldeira, K., Matsumoto, K., Munhoven, G., Montenegro, A., Tokos, K., 2009, Atmospheric lifetime of fossil fuel carbon dioxide: Annual Reviews of Earth and Planetary Science, v. 37, p. 117-34.

Bains, S., Corfield, R.M., Norris, R.D., 1999, Mechanisms of climate warming at the end of the Paleocene: Science, v. 285, p. 724-727.

Cao, L. Eby, M., Ridgwell, A., Caldeira, K., Archer, D., Ishida, A., Joos, F., Matsumoto, K., Mikolajewicz, U., Mouchet, A., Orr, J.C., Plattner, G.-K., Schlitzer, R., Tokos, K., Totterdell, I., Tschumi, T., Yamanaka, Y., Yool, A., 2009, The role of ocean transport in the uptake of anthropogenic CO_2: Biogeosciences, v. 6, p. 375–390.

Colbourn, G., Ridgwell, A., Lenton, T.M., 2013, The Rock Geochemical Model (RokGeM) v0.9: Geoscience Model Development, v. 6, p. 1543–1573.

Edwards, N.R., Marsh, R., 2005, Uncertainties due to transport-parameter sensitivity in an efficient 3-D ocean-climate model: Climate dynamics, v. 24, p. 415-433.

Gibbs, S.J., Stoll, H.M., Bown, P.R., Bralower, T.J., 2010, Ocean acidification and surface 235 water carbonate production across the Paleocene-Eocene thermal maximum: Earth and Planetary Science Letters, v. 295, p. 583-592.

Nunes, F., Norris, R.D., 2006, Abrupt reversal in ocean overturning during Paleocene-Eocene warm period: Nature, v. 439, p. 60-63.

Ridgwell, A., Hargreaves J.C., 2007, Regulation of atmospheric CO_2 by deep-sea sediments in an Earth system model: Global Biogeochemical Cycles, v. 21, GB2008, doi:10.1029/2006GB002764.

Ridgwell, A., Zondervan, I., Hargreaves, J. C., Bijma, J., Lenton, T.M., 2007, Assessing the potential long-term increase of fossil fuel uptake due to CO_2-calcification feedback: Biogeosciences, v. 4, p. 481–492.

Self-Trail, J.M., Powars, D.S., Watkins, D.K., and Wandless, G.A., 2012, Calcareous nannofossil assemblage changes across the Paleocene-Eocene Thermal Maximum: Evidence from a shelf setting: Marine Micropaleontology, v. 92-93, p. 61-80.

Tindall, J.R., Flecker, R., Valdes, P., Schmidt, D.N., Markwick, P., Harris, J., 2010, Modelling the oxygen isotope distribution of ancient seawater using a coupled ocean-atmosphere

GCM: Implications for reconstructing early Eocene climate: Earth and Planetary Science Letters, v. 292, p. 265-273.

References for Supplementary Figure DR1

a. Self-Trail, J.M., Powars, D.S., Watkins, D.K., Wandless, G.A., 2012, Calcareous nannofossil assemblage changes across the Paleocene-Eocene Thermal Maximum: Evidence from a shelf setting: Marine Micropaleontology, v. 92-93, p. 61-80.

b. Bybell, L.M., Self-Trail, J.M., 1994, Evolutionary, biostratigraphic, and taxonomic study of calcareous nannofossils from a continuous Paleocene-Eocene boundary section in New Jersey: U.S. Geol. Survey Prof. Paper 1554, U.S. Gov., Washington.

c. Gibbs, S.J., Bown, P.R., Sessa, J.A., Bralower, T.J., and Wilson, P.A., 2006, Nannoplankton extinction and origination across the Paleocene-Eocene thermal maximum: Science, v. 314, p. 1770-1773.

d. Gibbs, S.J., Bralower, T.J., Bown, P.R., Zachos, J.C., and Bybell, L.M., 2006, Shelf and open-ocean calcareous phytoplankton assemblages across the Paleocene-Eocene thermal maximum: implications for global productivity gradients: Geology, v. 34, p. 233-236.

e. Jiang, S., Wise Jr., S.W., 2006, Surface-water chemistry and fertility variations in the tropical Atlantic across the Paleocene/Eocene Thermal Maximum as evidenced by calcareous nannoplankton from ODP Leg 207, Hole 1259B: Revue de micropaleontology, v. 49, p. 227-244.

f. Mutterlose, J., Linnert, C., Norris, R., 2007, Calcareous nannofossils from the Paleocene-Eocene Thermal Maximum of the equatorial Atlantic (ODP Site 1260B): Evidence for tropical warming: Marine Micropaleontology, v. 65, p. 13-31.

g. Raffi, I., Backman, J., Zachos, J.C., Sluijs, A., 2006, The response of calcareous nannofossil assemblages to the Paleocene Eocene Thermal Maximum at the Walvis Ridge in the South Atlantic: Marine Micropaleontology, v. 70, p. 201-212.

h. Bralower, T., 2002, Evidence for surface water oligotrophy during the Paleocene-Eocene thermal maximum: nannofossil assemblage data from Ocean Drilling Program Site 690, Maud Rise, Weddell Sea: Paleoceanography, v. 17, p. 1023, doi:10.1029/2001PA000662.

i. Schmitz, B., Pujalte, V., 2007, Abrupt increase in seasonal extreme precipitation at the Paleocene-Eocene boundary: Geology, v. 35, p. 215-218.

j. Bernaola, G., et al., 2006, Biomagnetostratigraphic analysis of the Gorrondatze section (Basque Country, Western Pyrenees): its significance for the definition of the Ypresian/Lutetian boundary stratotype: Neues jahrbuch für geologie und palaontologie – anhandlungen, v. 241, p. 67-109.

k. Angori, E., Bernaola, G., Monechi, S., 2007, Calcareous nannofossil assemblages and their response to the Paleocene-Eocene Thermal Maximum event at different latitudes: ODP Site 690 and Tethyan sections: Geological Society of America Special Papers, v. 424, p. 69-85.

l. Angori, E., Monechi, S., 1996, High-resolution calcareous nannofossil biostratigraphy across the Paleocene/Eocene boundary at Caravaca (southern Spain): Israel Journal of Earth Sciences, v. 44, p. 197-206.

m. Agnini, C., Fornaciari, E., Rio, D., Tateo, F., Backman, J., Giusberti, L., 2007, Responses of calcareous nannofossil assemblages, mineralogy and geochemistry to the environmental perturbations across the Paleocene/Eocene boundary in the Venetian Pre-Alps: Marine Micropaleontology, v. 63, p. 19-38.

n. Tantawy, A.A., 2006, Calcareous nannofossils of the Paleocene-Eocene Transition at Qena Region, Central Nile Valley, Egypt: Marine Micropaleontology, v. 52, p. 193-222.

o. Bown, P., and Pearson, P., 2009, Calcareous plankton evolution and the Paleocene/Eocene thermal maximum event: new evidence from Tanzania. Marine Micropaleontology 71, 60-70.

p. Tremolada, F., Bralower, T.J., 2004, Nannofossil assemblage fluctuations during the Paleocene-Eocene Thermal Maximum at Sites 213 (Indian Ocean) and 401 (North Atlantic Ocean): palaeoceanographic implications: Marine Micropaleontology, v. 52, p. 107-116.

q. Jiang, S., Wise Jr., S.W., 2007, Abrupt turnover in calcareous-nannoplankton assemblages across the Paleocene/Eocene Thermal Maximum: implications for surface-water oligotrophy over the Kerguelen Plateau, Southern Indian Ocean: U.S. Geological Survey National Academy short research paper, v. 24, doi:10.3133/of2007-1047.srp024.